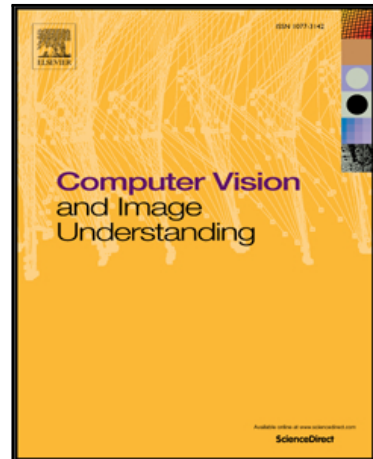


Accepted Manuscript

Human skin detection through correlation rules between the YCb and YCr subspaces based on dynamic color clustering

Nadia Brancati, Giuseppe De Pietro, Maria Frucci, Luigi Gallo

PII: S1077-3142(16)30198-9
DOI: [10.1016/j.cviu.2016.12.001](https://doi.org/10.1016/j.cviu.2016.12.001)
Reference: YCVIU 2517



To appear in: *Computer Vision and Image Understanding*

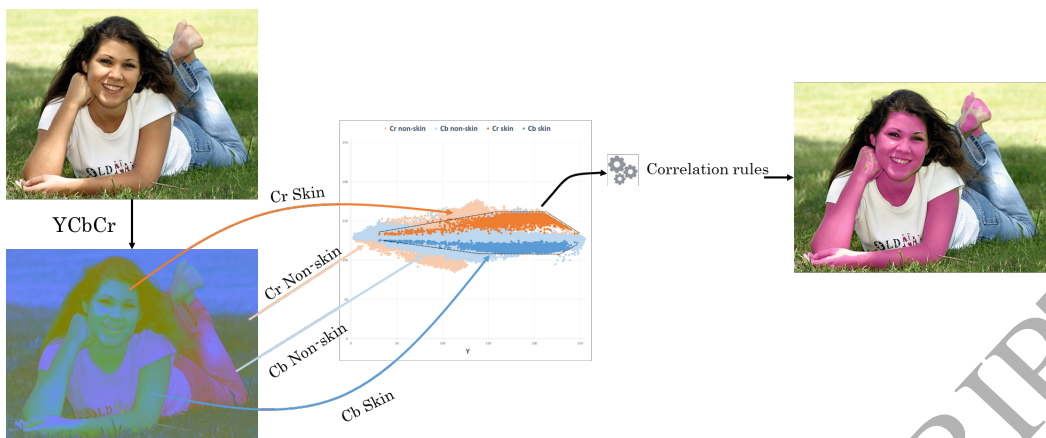
Received date: 2 February 2016
Revised date: 18 October 2016
Accepted date: 1 December 2016

Please cite this article as: Nadia Brancati, Giuseppe De Pietro, Maria Frucci, Luigi Gallo, Human skin detection through correlation rules between the YCb and YCr subspaces based on dynamic color clustering, *Computer Vision and Image Understanding* (2016), doi: [10.1016/j.cviu.2016.12.001](https://doi.org/10.1016/j.cviu.2016.12.001)

This is a PDF file of an unedited manuscript that has been accepted for publication. As a service to our customers we are providing this early version of the manuscript. The manuscript will undergo copyediting, typesetting, and review of the resulting proof before it is published in its final form. Please note that during the production process errors may be discovered which could affect the content, and all legal disclaimers that apply to the journal pertain.

Highlights

- Novel skin detection method based on correlation rules that evaluate the combinations of chrominance values to identify the skin pixels in the YCb and YCr subspaces
- Definition of a fitting model of skin-candidate pixels for the generation of image-specific trapezia in the YCb and YCr subspaces
- Comparisons with six well-known rule-based methods in literature show that the proposed method outperforms the others in terms of F-measure, Dprs and Precision



Human skin detection through correlation rules between the YCb and YCr subspaces based on dynamic color clustering

Nadia Brancati, Giuseppe De Pietro, Maria Frucci, Luigi Gallo

*Institute for High Performance Computing and Networking
National Research Council of Italy (ICAR-CNR), Naples, Italy
 {nadia.brancati, giuseppe.depietro, maria.frucci, luigi.gallo}@cnr.it}*

Abstract

This paper presents a novel rule-based skin detection method that works in the $YCbCr$ color space. The method is based on correlation rules that evaluate the combinations of chrominance values to identify the skin pixels in the YCb and YCr subspaces. The correlation rules depend on the shape and size of dynamically generated skin color clusters, which are computed on a statistical basis in the YCb and YCr subspaces for each single image, and represent the areas that include most of the candidate skin pixels. Comparisons with six well-known rule-based methods in literature carried out on four publicly available databases show that the proposed method outperforms the others in terms of quantitative performance evaluation parameters. Moreover, the qualitative analysis shows that the method achieves satisfactory results also in critical scenarios, including severe variations in illumination conditions.

Keywords: skin detection, $YCbCr$ color space, pixel based method, pixel classification, dynamic color clustering, correlation rules

1. Introduction

Skin detection is an important issue in color image processing, which has been extensively studied over the years. It is a useful technique for the detection, segmentation and tracking of human skin in images or video streams. The interest in skin detection algorithms derives from their applicability to a wide range of applications such as gesture recognition, video surveillance, ego-vision systems, human computer interaction [1], human activity recognition [2–4], nude images and video blocking [5, 6], and age estimation [7].

Skin pixels can vary depending on race, the global illumination of the scene, and the different illumination of skin areas in the same region. Many false positives can be generated when the background contains objects with a color similar to skin; moreover, many false negatives can be detected in correspondence with a human skin region at different illuminations. Since many applications, for example ego-vision systems, require the detection of human skin regions in video streams, recorded both indoors and outdoors, with high or low illumination condi-

tions, an important issue is to achieve a satisfactory and fast skin detection under uncontrolled lighting conditions.

There are three kinds of approach for skin detection: rule-based, machine learning and hybrid. They mainly differ in terms of classification rate and computational effort. Machine learning and hybrid methods require a training set, from which the decision rules are learned. Generally, such approaches outperform the rule-based methods, but require a large and representative training data set. Moreover, these methods require a long classification time, which usually excludes real-time applications. An effective optimization of the execution time can be obtained by building a look-up table once the classifier has been trained, even if this requires additional computations during the training phase. This is the main reason why several recent applications use rule-based skin detection methods [8–14]. In fact, rule-based approaches can provide satisfactory results in a wide range of applications with a reduced computational burden.

In this paper, we propose a dynamic rule-based

skin detection method in the YCbCr color space that proves to be robust against severe illumination variations. It takes advantage of the luminance information to obtain the chromatic ranges useful to classify the skin pixels. The method is based on correlation rules between the YCb and YCr subspaces, which take into account image-specific skin color clusters computed on a statistical basis. The clusters represent the sets of chrominance values that are associated to most of the skin pixels in the current image. The shape and the size of the clusters mainly depend on the lighting conditions and are identified on the basis of the information of luminance values Y in the current image. This approach makes our method robust to changes in lighting conditions, because it works on non-predefined clusters that are identified as image-specific skin color sets. The skin classification is based on the use of the correlation rules between the YCr and YCb subspaces that, depending on the shape and size of the clusters, evaluate the combinations of chrominance values to identify the skin pixels. Because of its generality, our method is suitable for use in every application that requires skin detection; moreover, it requires a low computational effort. The source code for the implementation of the algorithms presented in this paper is freely available at https://github.com/nadiabranicati/skin_detection/, for the repeatability of the results and further comparative evaluation with other skin detection techniques.

The rest of the paper is organized as follows: Section 2 summarizes the related work for skin detection; Section 3 describes in detail the proposed method; in Section 4, the comparative evaluation of the proposed method is presented and discussed; and finally, our conclusions are reported in Section 5.

2. Related Work

Extensive surveys on skin detection and segmentation in color images have been presented in [15–19]. In all the proposed approaches, one of the main issues is the definition of the optimal color space in which to work.

The main color spaces adopted for skin detection are RGB, HSV and YCbCr. RGB is the most commonly used color space for storing and representing digital images, since the data captured by a camera are normally provided as RGB signals. Such a color space corresponds to the three primary colors, red, green and blue, and it is strongly dependent

on the luminosity, which can be computed as the median of its components. In the HSV and YCbCr color spaces, the chrominance and luminance components are split. In particular, the HSV color space is obtained through a non-linear transformation from RGB; the components hue (H) and saturation (S) represent the chrominance, whereas the component value (V) represents the luminance. Similar color spaces are HSI, HSL, and TSV. In the YCbCr color space, Cb is the chrominance component obtained by subtracting the luminance component Y from B, while Cr is the chrominance component obtained by subtracting the luminance component Y from R.

Skin detection methods are of three kinds: machine learning, rule-based and hybrid. In machine learning approaches, the skin model can be defined from a training set of skin and non-skin classes. The most popular method is the Bayesian classifier. In [20] a Bayesian classifier in the RGB color space is proposed. Histograms for skin and non-skin classes are built, using a training database. Then, for the testing set, a pixel is classified as a skin or non-skin pixel, based on its probability, computed with a Bayes' rule. Non-parametric techniques require a large amount of training data, which in some cases may not cover all possible occurrences of skin color. Parametric approaches bypass this problem: they model the skin color either by using a Gaussian mixture model (GMM), transforming the RGB color space into a mono-dimensional space [21–23]. In [24], a survey of artificial neural networks or semi-parametric methods is presented. In [25] a skin detection method based on a multi-agent learning Bayesian classifier and a neural network in the RGB and YCbCr color spaces is presented.

Concerning the rule-based approaches, many studies operate in the HSV and YCbCr color spaces, some take into account the luminance component (see [26, 27] for the HSV space and [28–30] for the YCbCr space), while others ignore the luminance component (see [8, 31, 32] for the HSV space and [33–38] for the YCbCr space). However, some studies [21, 28, 29] have shown that the luminance component is important for a correct skin detection since it has been demonstrated that skin color is non-linearly dependent on the luminance in different color spaces. In [39], heuristic rules in the RGB color space, which also depend on the luminosity of the image, are used to detect skin regions. In [28], a skin color model is obtained by calculating the centers and spreads of the skin clusters in the YCb

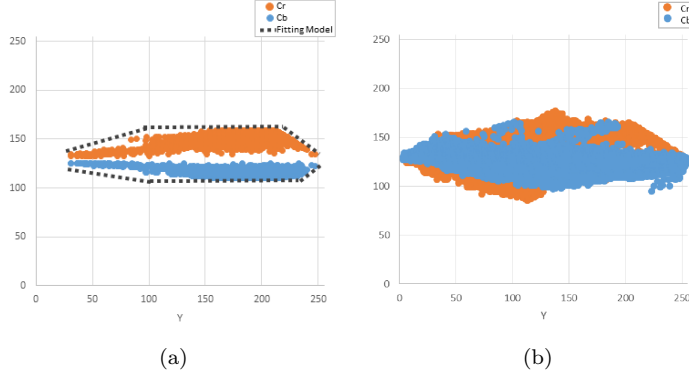


Figure 1: Cr and Cb component functions of the Y component (a) skin pixels only (b) skin and non-skin pixels.

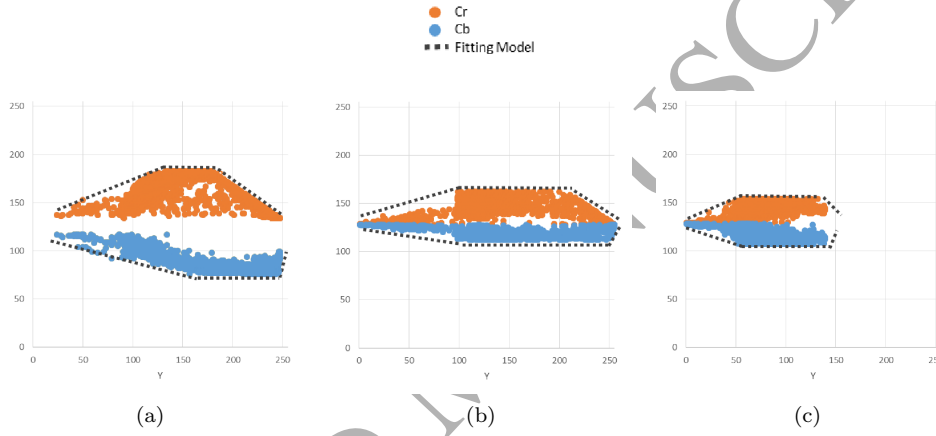


Figure 2: Fitting model for the YCb and YCr subspaces, in different conditions of illumination: (a) indoors with artificial light (b) outdoors with sunlight and (c) with low lighting.

and YCr subspaces. In these subspaces, the skin color cluster assumes a trapezoidal shape. Alternatively, a non-linear transformation of the $YCbCr$ color space is applied and in this case, the skin color cluster is represented as an ellipse in the new $CbCr$ subspace. A genetic algorithm that finds the optimal values to include in various rule-based skin detection approaches has been presented in [40].

Finally, there are some hybrid methods that combine different approaches [41–43]. In particular, a method based on a Multilayer Perceptron Artificial Neural Network combined with a k-means clustering, which takes advantage of the color and texture information of the skin regions, has recently been presented in [44].

3. The proposed method

At first, the conversion between the RGB color space and the $YCbCr$ color space is performed, by using the ITU-R BT.601-5 conversion [45].

The skin pixel clusters in the YCb and YCr subspaces, as shown in [28], exhibit a trapezoidal shape. Figure 1.a shows an example of skin pixel clusters in the $YCbCr$ color space considering only the skin pixels for a given image. A fitting model of the skin pixel sets shows the trapezoidal shape of the clusters in the YCb and YCr subspaces. For the same image, figure 1.b shows the color pixel distributions, where both the skin and non-skin pixels are included. We experimentally observed that the shape and the size of the trapezia, representing the distributions of the skin pixels in the image, change according to many factors, including the illumination conditions. To carry out such experiments,

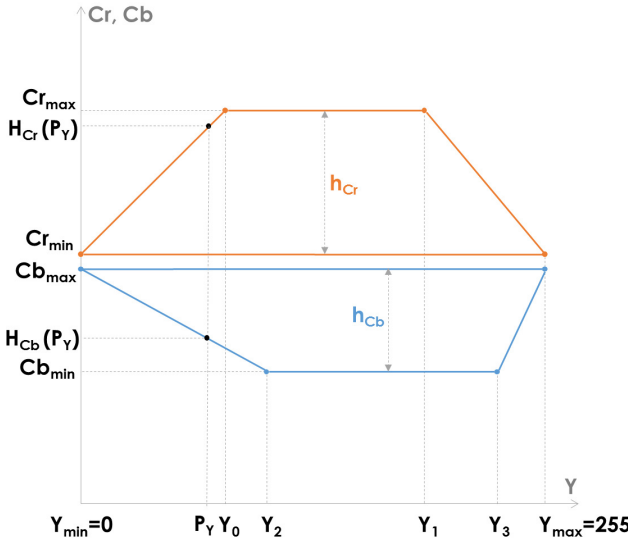


Figure 3: Graphical representation of Y_{min} , Y_{max} , Y_0 , Y_1 , Y_2 , Y_3 , Cr_{max} , Cr_{min} , Cb_{max} , Cb_{min} , h_{Cr} , h_{Cb} , $H_{Cr}(P_Y)$, $H_{Cb}(P_Y)$ parameters.

we have built a dataset of 50 color images where the ground truths of the skin regions were manually extracted. Such images were acquired in different lighting conditions: indoors with artificial light, outdoors with direct sunlight and with low lighting, and finally in the presence of a non-uniform lighting distribution. Taking into account the skin pixel distributions of the ground truths of the selected images, we observed that the bases of the trapezia representing the skin color clusters for acquisition in high illumination conditions are larger than those associated with the skin color clusters in low illumination conditions. Some examples of the skin pixel clusters in the YCb and YCr subspaces in different illumination conditions, together with the best achievable trapezoidal fittings, are shown in figure 2.

Moreover, we observed that the chrominance components of a skin pixel P with coordinates (P_Y, P_{Cb}, P_{Cr}) in the $YCbCr$ space exhibit the following behavior: the further is the (P_Y, P_{Cr}) point from the longer base of the trapezium in the YCr subspace, the further is the (P_Y, P_{Cb}) point from the longer base of the trapezium in the YCb subspace, and vice versa.

Starting from this observation, the proposed skin detection method is based on the definition of image-specific trapezia in the YCb and YCr subspaces [30], and on the verification of the correla-

tion rules between these subspaces that reflect the inversely proportional behavior of the chrominance components. For the sake of simplicity, we will refer to figure 3 for a description of the process for the detection of the image-specific trapezia in the subspaces YCb and YCr (T_{YCr} and T_{YCb} , in the following). Varying Y in the range $[Y_{min}, Y_{max}]$ with $Y_{min} = 0$ and $Y_{max} = 255$, the coordinates of points belonging to the longer bases of T_{YCr} and T_{YCb} are given by (Y, Cr_{min}) and (Y, Cb_{max}) in the YCr and YCb subspaces, respectively. The values of Cr_{min} and Cb_{max} have been selected by considering the minimum of Cr and the maximum of Cb , as reported in [33]. The coordinates of points belonging to the remaining sides of the trapezia are given by $[Y, H_{Cr}(Y)]$ and $[Y, H_{Cb}(Y)]$ with:

$$H_{Cr}(Y) = \begin{cases} Cr_{min} + h_{Cr} \left(\frac{Y - Y_{min}}{Y_0 - Y_{min}} \right) & Y \in [Y_{min}, Y_0[\\ Cr_{max} & Y \in [Y_0, Y_1] \\ Cr_{min} + h_{Cr} \left(\frac{Y - Y_{max}}{Y_1 - Y_{max}} \right) & Y \in]Y_1, Y_{max}] \end{cases}$$

$$H_{Cb}(Y) = \begin{cases} Cb_{min} + h_{Cb} \left(\frac{Y - Y_2}{Y_{min} - Y_2} \right) & Y \in [Y_{min}, Y_2[\\ Cb_{min} & Y \in [Y_2, Y_3] \\ Cb_{min} + h_{Cb} \left(\frac{Y - Y_3}{Y_{max} - Y_3} \right) & Y \in]Y_3, Y_{max}] \end{cases}$$

where $h_{Cr} = Cr_{max} - Cr_{min}$ and $h_{Cb} = Cb_{max} - Cb_{min}$ this being the heights of T_{YCr} and T_{YCb} , respectively.

The Cr_{max} value is computed by taking into account the histogram of the pixels with values of Cr in the range $[Cr_{min}, 183]$, looking for the maximum of Cr that is associated with at least 10% of the pixels in the image. In the same way, the Cb_{min} value is computed by taking into account the histogram of the pixels with values of Cb in the range $[77, Cb_{max}]$, looking for the minimum of Cb that is associated with at least 10% of the pixels in the image. The Y_0 and Y_1 values are respectively

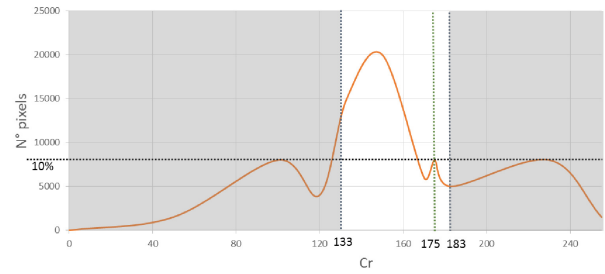


Figure 4: The calculus of Cr_{max} on the histogram of Cr values for a 320×240 image.

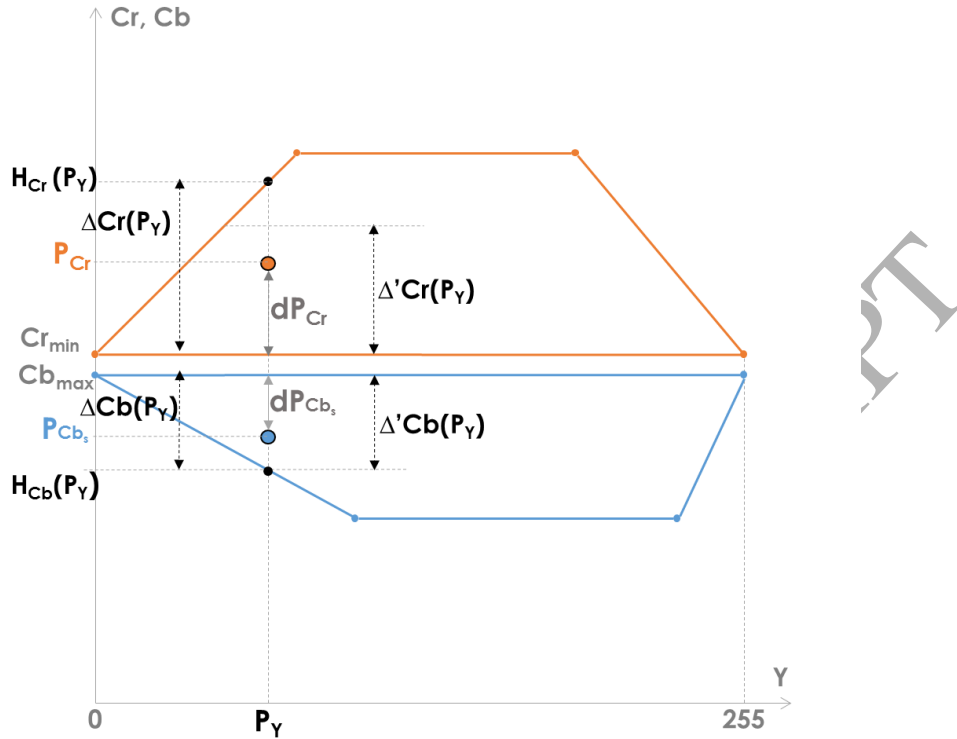


Figure 5: Graphical representation of $H_{Cr}(P_Y)$, $H_{Cb}(P_Y)$, dP_{Cr} , dP_{Cb_s} , $\Delta_{Cr}(P_Y)$, $\Delta'_{Cr}(P_Y)$, $\Delta_{Cb}(P_Y)$, $\Delta'_{Cb}(P_Y)$, P_{Cb_s} (in the case $Area_{T_{YCr}} \geq Area_{T_{YC_b}}$) parameters.

set as the 5th percentile and the 95th percentile of the luminance values associated with the pixels of the image with $Cr = Cr_{max}$ (see figure 4). The same procedure is used to find the Y_2 and Y_3 values considering the pixels with $Cb = Cb_{min}$.

The correlation rules between the chromatic components P_{Cr} and P_{Cb} of a pixel P are based on the computation of the following parameters:

- the minimum difference I_P between the values P_{Cr} and P_{Cb} ;
- an estimated value of P_{Cb} , namely P_{Cb_s} ;
- the maximum distance J_P between the points (P_Y, P_{Cb}) and (P_Y, P_{Cb_s}) .

On the basis of these parameters, a pixel P is classified as a skin pixel if both the following conditions hold:

$$P_{Cr} - P_{Cb} \geq I_P \quad (C.0)$$

$$|P_{Cb} - P_{Cb_s}| \leq J_P \quad (C.1)$$

The condition C.0 indicates that the chrominance components should be sufficiently far from each other, while the condition C.1 indicates the range of values delimiting the P_{Cb_s} value, to which the P_{Cb} should belong.

For the sake of simplicity, we will refer to figure 5 to explain the progress of the computation of the parameters I_P , P_{Cb_s} and J_P .

The estimated value of P_{Cb_s} is set equal to:

$$P_{Cb_s} = Cb_{max} - dP_{Cb_s}$$

where dP_{Cb_s} is the distance between the points with coordinates (P_Y, P_{Cb_s}) and (P_Y, Cb_{max}) in the YC_b subspace. On the basis of the inversely proportional behavior of the chrominance components observed within the trapezia, the value of the dP_{Cb_s} is proportionally computed with respect to the distance $dP_{Cr} = P_{Cr} - Cr_{min}$ between the points with coordinates (P_Y, P_{Cr}) and (P_Y, Cr_{min}) in the YCr subspace:

$$dP_{Cb_s} = \alpha \cdot dP_{Cr}$$

where α takes into account the different shapes of

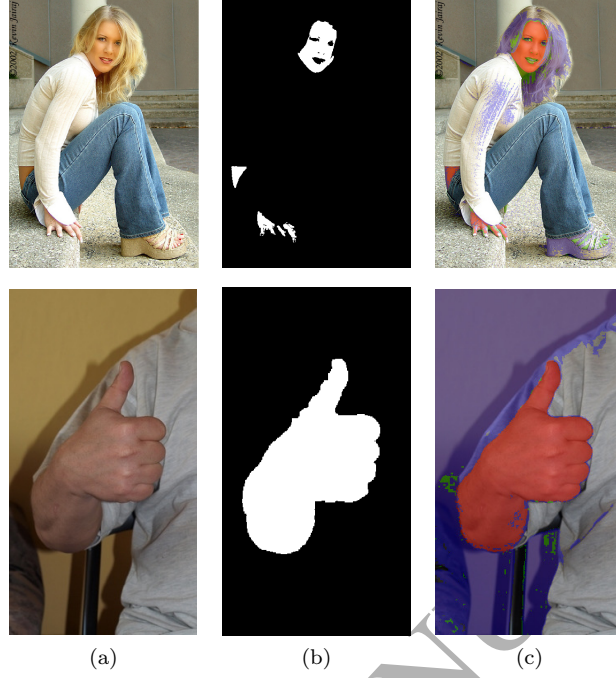


Figure 6: (a) the input image; (b) the ground truth; (c) the input image in which are highlighted: in orange, those pixels that satisfy both the C.0 and C.1 condition and belong to the foreground of the ground truth; in green, those pixels that satisfy both the C.0 and C.1 conditions but belong to the background of the ground truth; and, in violet, those pixels that satisfy only the C.0 condition.

the trapezia, being computed as the ratio between the normalized heights of the two trapezia in correspondence with the current luminance value P_Y .

Precisely, the distances $\Delta_{Cr}(P_Y)$ and $\Delta_{Cb}(P_Y)$ between the points $(P_Y, H_{Cr}(P_Y))$ and $(P_Y, H_{Cb}(P_Y))$ and the longer base of their respective trapezia are first computed:

$$\Delta_{Cr}(P_Y) = H_{Cr}(P_Y) - Cr_{min}$$

$$\Delta_{Cb}(P_Y) = Cb_{max} - H_{Cb}(P_Y)$$

Now, the values of $\Delta_{Cr}(P_Y)$ and of $\Delta_{Cb}(P_Y)$ are normalized with respect to the difference in size of the trapezia:

$$\Delta'_{Cr}(P_Y) = \begin{cases} \Delta_{Cr}(P_Y) \cdot \frac{A_{T_{YCb}}}{A_{T_{YCr}}} & \text{if } A_{T_{YCr}} \geq A_{T_{YCb}} \\ \Delta_{Cr}(P_Y) & \text{otherwise} \end{cases}_{260}$$

$$\Delta'_{Cb}(P_Y) = \begin{cases} \Delta_{Cb}(P_Y) & \text{if } A_{T_{YCr}} \geq A_{T_{YCb}} \\ \Delta_{Cb}(P_Y) \cdot \frac{A_{T_{YCr}}}{A_{T_{YCb}}} & \text{otherwise} \end{cases}$$

where $A_{T_{YCr}}$ and $A_{T_{YCb}}$ are the areas of the trapezia T_{YCr} and T_{YCb} , respectively. 265

Then, the value α is given by:

$$\alpha = \frac{\Delta'_{Cb}(P_Y)}{\Delta'_{Cr}(P_Y)}$$

Finally, I_P and J_P are given by:

$$I_P = sf \cdot [(\Delta'_{Cr}(Y) - dP_{Cr}) + (\Delta'_{Cb}(Y) - dP_{Cb_s})]$$

and

$$J_P = dP_{Cb_s} \cdot \frac{dP_{Cb_s} + dP_{Cr}}{\Delta'_{Cb}(Y) + \Delta'_{Cr}(Y)}$$

with

$$sf = \frac{\min((Y_1 - Y_0), (Y_3 - Y_2))}{\max((Y_1 - Y_0), (Y_3 - Y_2))}$$

Figure 6 shows the effects of the application of the two formulae C.0 and C.1. In more detail, in figure 6.c, the pixels that satisfy the C.0 rule are highlighted in violet, orange or green. With the exception of the violet ones, the highlighted pixels satisfy also the C.1 rule. In particular, the pixels highlighted in orange are also present in the foreground of the ground truth. Differently, the pixels highlighted in green satisfy both the C.0 and C.1 conditions, but belong to the background of the

ground truth. The C.0 rule provides a first, coarse-grained classification of skin pixels considering the minimum distance between the P_{Cr} and P_{Cb} values, according to the P_Y value. Basically, the C.0 rule is generally satisfied by skin-colour like pixels. Next, the C.1 rule provides a fine-grained refinement. In fact, this rule is satisfied only by those pixels that show an inversely proportional behavior of their chrominance components.

4. Comparative evaluation

4.1. Results

The proposed method has been compared with six rule-based methods which are among the most used in recent literature [8–14]: method [28] in its two different formulations (the YCbCr space and CbCr subspace); methods [33] and [37], that work in the CbCr subspace; method [39], that works in the RGB color space; and method [31], in the HSV color space. We selected these methods because, similarly to the proposed approach, they classify skin pixels by taking into account only the color information. Moreover, in recent literature skin detection techniques have been compared with some of these methods [46].

Comparative evaluations have been carried out on four publicly available databases. In particular, we have used Hand Gesture Recognition (HGR) [47, 48], ECU [49], Pratheepan [50], and Compaq [20]. The total number of the examined images is 10,306.

Some results of the methods for the HGR, ECU, Pratheepan and Compaq databases are reported in figures 7, 8, 9, 10, respectively. Some critical scenarios with complex backgrounds and at different illumination conditions, are shown in figure 11.

To carry out a quantitative evaluation of the performance of the proposed method, we used the measurements of Precision (PR), Recall (RE), Specificity (SP), F-Measure [51] and D_{prs} [52]. By denoting as TP the number of pixels correctly classified as skin pixels, as TN the number of non-skin pixels correctly classified as non-skin pixels, as FP the number of non-skin pixels wrongly classified as skin pixels, and as FN the number of skin pixels wrongly classified as non-skin pixels, the above measurements are computed as follows:

$$PR = \frac{TP}{TP + FP}$$

$$RE = \frac{TP}{TP + FN}$$

$$SP = \frac{TN}{TN + FP}$$

$$F - Measure = \frac{2PR \times RE}{PR + RE}$$

$$D_{prs} = \sqrt{(1 - PR)^2 + (1 - RE)^2 + (1 - SP)^2}$$

Except for D_{prs} , that represents a distance from the ground truth, all the values of these measurements should be maximized for a good performance of the method. The results using the different methods are reported in table 2.

For the sake of completeness, the results of the same methods on the 8,968 non-skin images of the Compaq database are reported in table 3. In this case, the Specificity, which measures the number of non-skin pixels that are correctly identified, was computed.

The performance of the algorithm was evaluated on a standard PC equipped with an Intel Xeon E5-2623 at 3 GHz, and with 16 GB RAM. For an image with a 320x400 resolution the execution time was, on average, 10 ms. The execution times of the single steps of the algorithm are reported in table 1.

4.2. Discussion

The objective of this work was to design a fast rule-based skin detector, which exhibits certain features, namely that it should be:

- generally suitable for use in different application domains;
- efficient even in the presence of severe variations in illumination conditions;
- computationally efficient, suitable for use also in near-real time applications.

The evaluation metrics considered in the experimental comparison, in particular Precision, Recall and Specificity, highlight different aspects of the detection algorithms. The F-measure instead, takes into account both Precision and Recall. The D_{prs} ,

Step	Operation	Avg (ms)
1	Setting of Cb_{max} and Cr_{min} with fixed values	0
2	Computation of Cb_{min} and Cr_{max}	2
3 and 4	Computation of A, B, C, D	2
5	Classification of a pixel as belonging to skin	6
		Total
		10

Table 1: Execution times of the single steps of the algorithm.

Measurement	Method	HGR	ECU	Pratheepan	Compaq	Overall
F-Measure	Hsu et al. in the YCbCr space [28]	0.3078	0.3829	0.3888	0.3105	0.3504
	Hsu et al. in the CbCr space [28]	0.5814	0.5308	0.5585	0.4312	0.5357
	Chai, Ngan [33]	0.7967	0.6059	0.5480	0.4373	0.6063
	Basilio et al. [37]	0.7913	0.6239	0.6170	0.4935	0.6372
	Kovac et al. [39]	0.5834	0.6572	0.6047	0.5557	0.6033
	Sobottka et al. [31]	0.6963	0.5444	0.5450	0.4691	0.5663
	Proposed Method	0.8252	0.6550	0.6592	0.5650	0.6902
Recall	Hsu et al. in the YCbCr space [28]	0.9822	0.8132	0.8582	0.7998	0.8436
	Hsu et al. in the CbCr space [28]	0.4958	0.5634	0.6011	0.5476	0.5520
	Chai, Ngan [33]	0.9820	0.9446	0.9494	0.8669	0.9357
	Basilio et al. [37]	0.9176	0.8457	0.9009	0.8026	0.8667
	Kovac et al. [39]	0.7551	0.7726	0.6258	0.6768	0.7076
	Sobottka et al. [31]	0.8353	0.7113	0.7808	0.7034	0.7577
	Proposed Method	0.7664	0.7181	0.8199	0.8046	0.7772
Precision	Hsu et al. in the YCbCr space [28]	0.1825	0.2504	0.2306	0.1926	0.2215
	Hsu et al. in the CbCr space [28]	0.7025	0.5016	0.5215	0.3556	0.5203
	Chai, Ngan [33]	0.6702	0.4460	0.3852	0.2924	0.4484
	Basilio et al. [37]	0.6955	0.4942	0.4691	0.3563	0.5038
	Kovac et al. [39]	0.4753	0.5717	0.5849	0.4713	0.5258
	Sobottka et al. [31]	0.5969	0.4409	0.4186	0.3519	0.4520
	Proposed Method	0.8938	0.6021	0.5513	0.4354	0.6206
Specificity	Hsu et al. in the YCbCr space [28]	0.1873	0.4099	0.4225	0.3697	0.3474
	Hsu et al. in the CbCr space [28]	0.9488	0.8811	0.7702	0.8552	0.8638
	Chai, Ngan [33]	0.7543	0.6635	0.5781	0.5860	0.6455
	Basilio et al. [37]	0.7912	0.7597	0.7007	0.7062	0.7395
	Kovac et al. [39]	0.8806	0.8511	0.8955	0.8880	0.8788
	Sobottka et al. [31]	0.7691	0.7612	0.6844	0.7506	0.7413
	Proposed Method	0.9274	0.8716	0.8230	0.8046	0.8566
D_{prs}	Hsu et al. in the YCbCr space [28]	1.1556	0.9721	0.9704	1.043	1.028
	Hsu et al. in the CbCr space [28]	0.6253	0.6734	0.6414	0.8005	0.6703
	Chai, Ngan [33]	0.4215	0.6505	0.7508	0.8305	0.6588
	Basilio et al. [37]	0.4148	0.5810	0.6215	0.7346	0.5761
	Kovac et al. [39]	0.6274	0.5244	0.5780	0.6297	0.5701
	Sobottka et al. [31]	0.5184	0.6730	0.7020	0.7551	0.6525
	Proposed Method	0.2667	0.5043	0.5149	0.6286	0.4786

Table 2: Comparisons between the considered methods in terms of F-Measure, Recall, Precision, Specificity and D_{prs} .

defined as the Euclidean distance between the segmented image and the ground truth, takes into account both Precision, Recall and Specificity, providing an average and so a general measure of the efficiency of the skin detector.

Table 2 shows that the proposed method outperforms, overall, the other methods in terms of the F-measure. Considering the results obtained on the single datasets, the proposed method achieved the best score on Compaq, Pratheepan and HGR. On ECU, it achieved the second best score (0.22% lower than the best). Concerning the D_{prs} , the proposed method achieved the best score in all the considered databases.

Moreover, it must be emphasized that the other methods are unstable, showing good results for some measurements on specific databases and poor results for the same measurements on other databases. For example, method [33] shows a high F-Measure for the HGR database, but an F-Measure among the worst for the Pratheepan and Compaq databases. Method [39] shows the best re-

sults for Precision on both Pratheepan and Compaq databases, while it presents a low value for the HGR database. The proposed method, independently of the chosen database and the type of measurement, is always positioned among the best, either in first place or only very slightly lower than the first place.

In fact, the overall results presented in the last column of table 2, show that the proposed method is the best for F-Measure, Precision and D_{prs} , with an average score about 6%, 10% and 10% better than the second classified method, respectively.

Method	Specificity
Hsu et al. in the YCbCr space [28]	0.3401
Hsu et al. in the CbCr space [28]	0.8073
Chai, Ngan [33]	0.6762
Basilio et al. [37]	0.7638
Kovac et al. [39]	0.7897
Sobottka et al. [31]	0.7846
Proposed Method	0.8673

Table 3: Specificity for a set of non-skin images of the Compaq database.

As regard the Specificity, the proposed method obtained the third best score (2% lower than the first classified method in overall results). The Recall of the proposed method is significantly lower than the other methods. This aspect is due to the generally reduction of the false positives, at the expense of the true positives.

Concerning the non-skin images, the results reported in table 3 show that the proposed method outperforms the others when skin is not present in the image, with 86.73% of pixels correctly classified as non skin (6% more than the second ranked method).

The qualitative analysis shows that the proposed method provides satisfactory results on all the considered databases. The results achieved by using the six skin detection methods on selected images of the HGR, ECU, Pratheepan and Compaq databases are shown in figures 7, 8, 9, 10, respectively. In particular, in the HGR database, which essentially includes images acquired in low lighting conditions, the proposed method outperforms the other approaches. In the ECU, Compaq and Pratheepan databases, the application of the proposed method results in an improved skin detection in all those images in which high or low lighting conditions are present. In particular, the results for some critical scenarios are shown in figure 11, where different illumination conditions and skin-like objects, such as blonde hair, sand or wood, are present. In these cases, the proposed method outperforms the others.

5. Conclusions

We have presented a novel method for skin detection that works in the YCbCr color space. Such a method is based on the correlation rules between the YCb and YCr subspaces and takes into account dynamically defined skin cluster ranges, considering also the luminance component.

The performance of the proposed method has been tested on four publicly available databases, for a total of 10,306 images, producing satisfactory results both qualitatively and in terms of quantitative performance evaluation parameters such as Precision, Specificity, F-Measure and D_{prs} . Comparisons have been carried out with six other rule-based methods widely used in recent literature, demonstrating the generally higher performance of the proposed method.

References

- [1] Y. Zhu, G. Xu, D. J. Kriegman, A real-time approach to the spotting, representation, and recognition of hand gestures for human-computer interaction, Computer Vision and Image Understanding 85 (3) (2002) 189–208.
- [2] L. Baraldi, F. Paci, G. Serra, L. Benini, R. Cucchiara, Gesture recognition in ego-centric videos using dense trajectories and hand segmentation, in: IEEE Conference on Computer Vision and Pattern Recognition Workshops (CVPRW), IEEE, 2014, pp. 702–707.
- [3] C. Li, K. M. Kitani, Pixel-level hand detection in ego-centric videos, in: Computer Vision and Pattern Recognition (CVPR), 2013 IEEE Conference on, IEEE, 2013, pp. 3570–3577.
- [4] A. Betancourt, A sequential classifier for hand detection in the framework of egocentric vision, in: IEEE Conference on Computer Vision and Pattern Recognition Workshops (CVPRW), IEEE, 2014, pp. 600–605.
- [5] J. Stöttinger, A. Hanbury, C. Liensberger, R. Khan, Skin paths for contextual flagging adult videos, in: Advances in Visual Computing, Springer, 2009, pp. 303–314.
- [6] L. Zhao, J. Zhang, Y. Zhao, S. Zhao, Compressed domain based pornographic image recognition using multi-cost sensitive decision trees, Signal Processing 93 (8) (2013) 2126–2139.
- [7] K. Luu, T. D. Bui, C. Y. Suen, K. Ricanek, Spectral regression based age determination, in: IEEE Computer Society Conference on Computer Vision and Pattern Recognition Workshops (CVPRW), IEEE, 2010, pp. 103–107.
- [8] J.-M. Guo, Y.-F. Liu, C.-H. Chang, H.-S. Nguyen, Improved hand tracking system, IEEE Transactions on Circuits and Systems for Video Technology 22 (5) (2012) 693–701.
- [9] H. Liang, Y. Zhao, J. Wei, D. Quan, R. Cheng, Y. Wei, Robust hand detection and tracking based on monocular vision, in: Sixth International Conference on Intelligent Human-Machine Systems and Cybernetics (IHMSC), Vol. 2, IEEE, 2014, pp. 134–137.
- [10] S. Boucenna, P. Gaussier, P. Andry, L. Hafemeister, A robot learns the facial expressions recognition and face/non-face discrimination through an imitation game, International Journal of Social Robotics 6 (4) (2014) 633–652.
- [11] M. Ilbeygi, H. Shah-Hosseini, A novel fuzzy facial expression recognition system based on facial feature extraction from color face images, Engineering Applications of Artificial Intelligence 25 (1) (2012) 130–146.
- [12] H.-S. Yeo, B.-G. Lee, H. Lim, Hand tracking and gesture recognition system for human-computer interaction using low-cost hardware, Multimedia Tools and Applications 74 (8) (2013) 2687–2715.
- [13] Z. Wang, Hardware implementation for a hand recognition system on fpga, in: 5th International Conference on Electronics Information and Emergency Communication (ICEIEC), IEEE, 2015, pp. 34–38.
- [14] S. Asteriadis, K. Karpouzis, S. Kollias, Visual focus of attention in non-calibrated environments using gaze estimation, International Journal of Computer Vision 107 (3) (2014) 293–316.
- [15] M. Kawulok, J. Nalepa, J. Kawulok, Skin detection and segmentation in color images, in: Advances in Low-

- Level Color Image Processing, Springer, 2014, pp. 329–366.
- [16] P. Kakumanu, S. Makrogiannis, N. Bourbakis, A survey of skin-color modeling and detection methods, *Pattern recognition* 40 (3) (2007) 1106–1122.
- [17] S. L. Phung, A. Bouzerdoum, D. Chai, Skin segmentation using color pixel classification: analysis and comparison, *IEEE Transactions on Pattern Analysis and Machine Intelligence* 27 (1) (2005) 148–154.
- [18] K. B. Shaik, P. Ganesan, V. Kalist, B. Sathish, J. M. M. Jenitha, Comparative study of skin color detection and segmentation in HSV and YCbCr color space, *Procedia Computer Science* 57 (2015) 41–48.
- [19] S. J. Schmugge, S. Jayaram, M. C. Shin, L. V. Tsap, Objective evaluation of approaches of skin detection using roc analysis, *Computer Vision and Image Understanding* 108 (1) (2007) 41–51.
- [20] M. J. Jones, J. M. Rehg, Statistical color models with application to skin detection, *International Journal of Computer Vision* 46 (1) (2002) 81–96.
- [21] A. Cheddad, J. Condell, K. Curran, P. Mc Kevitt, A skin tone detection algorithm for an adaptive approach to steganography, *Signal Processing* 89 (12) (2009) 2465–2478.
- [22] P. Yogarajah, J. Condell, K. Curran, P. McKevitt, A. Cheddad, A dynamic threshold approach for skin tone detection in colour images, *International Journal of Biometrics* 4 (1) (2012) 38–55.
- [23] S. Jairath, S. Bharadwaj, M. Vatsa, R. Singh, Adaptive skin color model to improve video face detection, in: *Machine Intelligence and Signal Processing*, Springer, 2016, pp. 131–142.
- [24] H. K. Al-Mohair, J. Mohamad-Saleh, S. A. Suandi, Human skin color detection: a review on neural network perspective, *International Journal of Innovative Computing Information and Control* 8 (12) (2012) 8115–8131.
- [25] A. Zaidan, N. N. Ahmad, H. A. Karim, M. Larbani, B. Zaidan, A. Sali, Image skin segmentation based on multi-agent learning bayesian and neural network, *Engineering Applications of Artificial Intelligence* 32 (2014) 136–150.
- [26] S. Tsekridou, I. Pitas, Facial feature extraction in frontal views using biometric analogies, in: Proc. of EU-SIPCO, Vol. 98, 1998, pp. 315–318.
- [27] S. M. Dominguez, T. Keaton, A. H. Sayed, A robust finger tracking method for multimodal wearable computer interfacing, *IEEE Transactions on Multimedia* 8 (5) (2006) 956–972.
- [28] R.-L. Hsu, M. Abdel-Mottaleb, A. K. Jain, Face detection in color images, *IEEE Transactions on Pattern Analysis and Machine Intelligence* 24 (5) (2002) 696–706.
- [29] I. Hwang, S. H. Lee, B. Min, N. I. Cho, Luminance adapted skin color modeling for the robust detection of skin areas, in: *IEEE International Conference on Image Processing*, IEEE, 2013, pp. 2622–2625.
- [30] N. Brancati, M. Frucci, G. De Pietro, L. Gallo, Dynamic clustering for skin detection in YCbCr colour space, Tech. rep., Minsk: Publishing Center of Belarusian State University (2016).
- [31] K. Sobottka, I. Pitas, A novel method for automatic face segmentation, facial feature extraction and tracking, *Signal processing: Image communication* 12 (3) (1998) 263–281.
- [32] N. H. Dardas, N. D. Georganas, Real-time hand gesture detection and recognition using bag-of-features and support vector machine techniques, *IEEE Transactions on Instrumentation and Measurement* 60 (11) (2011) 3592–3607.
- [33] D. Chai, K. N. Ngan, Face segmentation using skin-color map in videophone applications, *IEEE Transactions on Circuits and Systems for Video Technology* 9 (4) (1999) 551–564.
- [34] C. Liensberger, J. Stöttinger, M. Kampel, Color-based and context-aware skin detection for online video annotation, in: *IEEE International Workshop on Multimedia Signal Processing (MMSP)*, IEEE, 2009, pp. 1–6.
- [35] R. Khan, J. Stöttinger, M. Kampel, An adaptive multiple model approach for fast content-based skin detection in on-line videos, in: *Proc. of the 1st ACM workshop on Analysis and retrieval of events/actions and workflows in video streams*, ACM, 2008, pp. 89–96.
- [36] M. Alsoos, A. Joukhadar, Posture independent model for hand detection and tracking, in: *Human-Computer Systems Interaction: Backgrounds and Applications* 3, Springer, 2014, pp. 301–312.
- [37] J. A. M. Basilio, G. A. Torres, G. S. Pérez, L. K. T. Medina, H. M. P. Meana, Explicit image detection using ycbcr space color model as skin detection, *Applications of Mathematics and Computer Engineering* (2011) 123–128.
- [38] S. Bilal, R. Akmelawati, M. J. E. Salami, A. A. Shafie, Dynamic approach for real-time skin detection, *Journal of Real-Time Image Processing* 10 (2) (2015) 371–385.
- [39] J. Kovac, P. Peer, F. Solina, Human skin color clustering for face detection, in: *EUROCON*, IEEE, 2003.
- [40] F. Gasparini, S. Corchs, R. Schettini, Recall or precision-oriented strategies for binary classification of skin pixels, *Journal of electronic imaging* 17 (2) (2008) 023017–023017.
- [41] A. Zaidan, N. Ahmed, H. A. Karim, G. M. Alam, B. Zaidan, Increase reliability for skin detector using backpropagation neural network and heuristic rules based on ycbcr, *Sci. Res. Essays* 5 (19) (2010) 2931–2946.
- [42] M. Chihaoui, A. Elkefi, W. Bellil, C. B. Amar, A novel face recognition system based on skin detection, hmm and lbp, *International Journal of Computer Science and Information Security* 14 (6) (2016) 308.
- [43] S. Yadav, N. Nain, A novel approach for face detection using hybrid skin color model, *Journal of Reliable Intelligent Environments* (2016) 1–14.
- [44] H. K. Al-Mohair, J. M. Saleh, S. A. Suandi, Hybrid human skin detection using neural network and k-means clustering technique, *Applied Soft Computing* 33 (2015) 337–347.
- [45] ITU-R BT.601-5 conversion, https://www.itu.int/dms_pubrec/itu-r/rec/bt/R-REC-BT.601-5-199510-S!!PDF-E.pdf.
- [46] L. Huang, W. Ji, Z. Wei, B.-W. Chen, C. C. Yan, J. Nie, J. Yin, B. Jiang, Robust skin detection in real-world images, *Journal of Visual Communication and Image Representation* 29 (2015) 147–152.
- [47] Database for hand gesture recognition, <http://sun.aei.polsl.pl/~mkawulok/gestures/>.
- [48] M. Kawulok, J. Kawulok, J. Nalepa, Spatial-based skin detection using discriminative skin-presence features, *Pattern Recognition Letters* 41 (2014) 3–13.
- [49] Face and skin detection database, <http://www.uow.edu.au/~jason/faces.html>.

- edu.au/~phung/download.html.
[50] Human skin detection dataset, http://web.fsktm.um.edu.my/~cschan/downloads_skin_dataset.html.
- [51] D. M. Powers, Evaluation: from precision, recall and f-measure to ROC, informedness, markedness and correlation, Journal of Machine Learning Technologies 2 (1) (2011) 37–63.
- [52] K. Intawong, M. Scuturici, S. Miguet, A new pixel-based quality measure for segmentation algorithms integrating precision, recall and specificity, in: Computer Analysis of Images and Patterns, Springer, 2013, pp. 188–195.

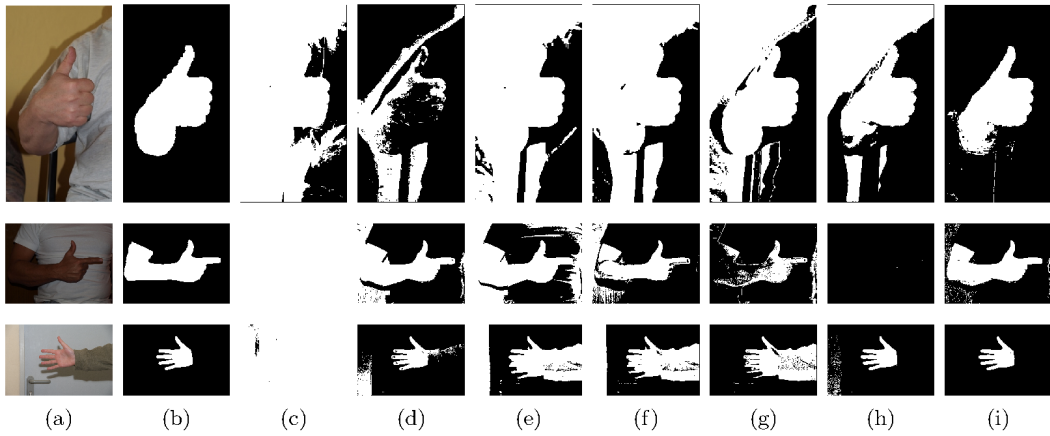


Figure 7: Skin detection results on the HGR database: (a) the input image; (b) the ground truth; (c) Hsu et al. in the YCbCr space [28] (2002); (d) Hsu et al. in the CbCr subspace [28] (2002); (e) Chai, Ngan [33] (1999); (f) Basilio et al. [37] (2011); (g) Sobottka et al. [31] (1998); (h) Kovac et al. [39] (2003); and (i) the proposed method.

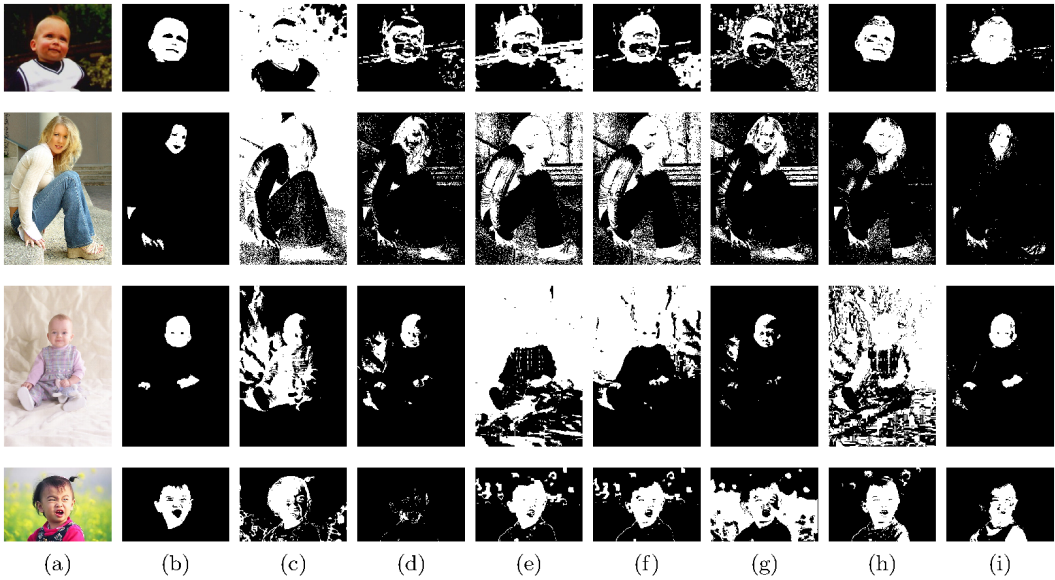


Figure 8: Skin detection results on the ECU database: (a) the input image; (b) the ground truth; (c) Hsu et al. in the YCbCr space [28] (2002); (d) Hsu et al. in the CbCr subspace [28] (2002); (e) Chai, Ngan [33] (1999); (f) Basilio et al. [37] (2011); (g) Sobottka et al. [31] (1998); (h) Kovac et al. [39] (2003); and (i) the proposed method.

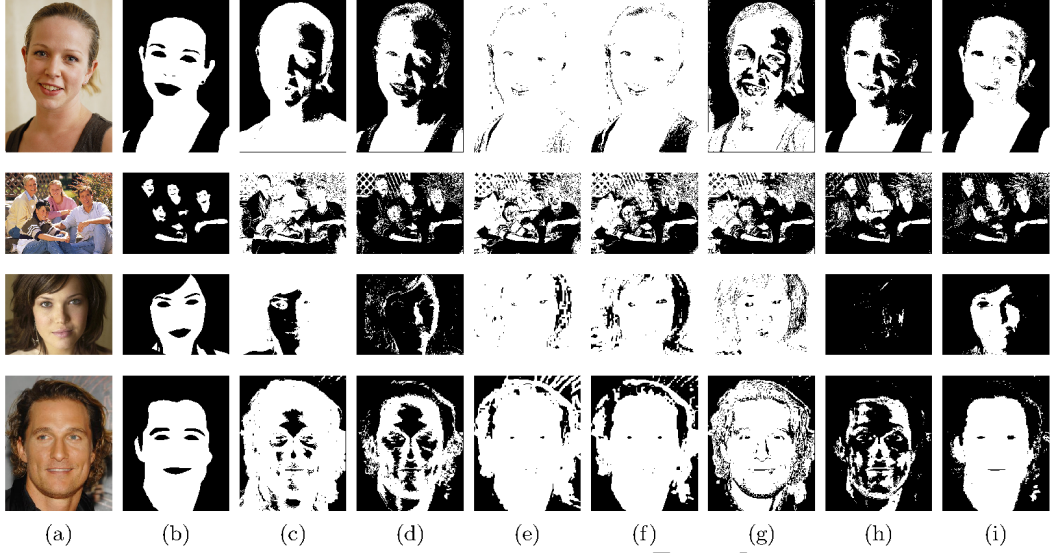


Figure 9: Skin detection results on the Pratheeepan database: (a) the input image; (b) the ground truth; (c) Hsu et al. in the YCbCr space [28] (2002); (d) Hsu et al. in the CbCr subspace [28] (2002); (e) Chai, Ngan [33] (1999); (f) Basilio et al. [37] (2011); (g) Sobottka et al. [31] (1998); (h) Kovac et al. [39] (2003); and (i) the proposed method.

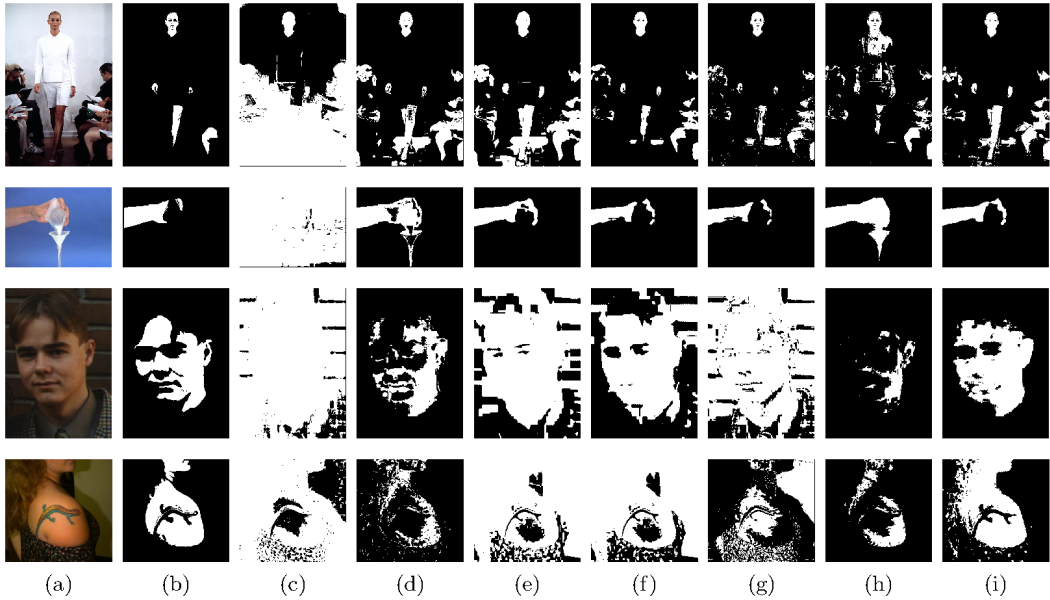


Figure 10: Skin detection results on the Compaq database: (a) the input image; (b) the ground truth; (c) Hsu et al. in the YCbCr space [28] (2002); (d) Hsu et al. in the CbCr subspace [28] (2002); (e) Chai, Ngan [33] (1999); (f) Basilio et al. [37] (2011); (g) Sobottka et al. [31] (1998); (h) Kovac et al. [39] (2003); and (i) the proposed method.



Figure 11: Skin detection results for critical scenarios: (a) the input image; (b) the ground truth; (c) Hsu et al. in the YCbCr space [28] (2002); (d) Hsu et al. in the CbCr subspace [28] (2002); (e) Chai, Ngan [33] (1999); (f) Basilio et al. [37] (2011); (g) Sobottka et al. [31] (1998); (h) Kovac et al. [39] (2003); and (i) the proposed method.